

Quantum Machine Learning Corrects Classical Force Fields: Stretching DNA Base Pairs in Explicit Solvent

Joshua T. Berryman*,¹ Amirhossein Taghavi,¹ Florian Mazur,^{1, a)} and Alexandre Tkatchenko¹

Department of Physics and Materials Science, University of Luxembourg, L-1511 Luxembourg City, Luxembourg.

(*Electronic mail: josh.berryman@uni.lu)

(Dated: 30 March 2022)

In order to improve the accuracy of molecular dynamics simulations, classical force fields are supplemented with a kernel-based machine learning method trained on quantum-mechanical fragment energies. As an example application, a potential-energy surface is generalised for a small DNA duplex, taking into account explicit solvation and long-range electron exchange–correlation effects. Study of the corrected potential energy versus extension shows that leading classical DNA models have excessive stiffness with respect to stretching. This discrepancy is found to be common across multiple forcefields. The quantum correction is in qualitative agreement to the experimental thermodynamics for larger DNA double helices, providing a candidate explanation for the general and long-standing discrepancy between single molecule stretching experiments and classical calculations of DNA stretching. The new dataset of quantum calculations and the associated Kernel Modified Molecular Dynamics (KMMD) method should be of general utility in biomolecular simulations. KMMD is made available as part of the AMBER22 simulation software.

I. INTRODUCTION

The dominant long-range interactions in molecular systems can be treated classically with great efficiency as a pairwise Coulomb term ($U_c \propto 1/r$) plus a pairwise fluctuating dipole-dipole attraction (a dispersion interaction, $U_d \propto 1/r^6$), with atoms represented as spheres having fitted non-integer charge and attraction parameters, both of which in theory can be derived from *ab initio* quantum mechanics.^{1–3} Limitations to the accuracy of this approach are especially evident when atomic polarisability is anisotropic, or when the atoms are part of a flexible molecule in which the atomic polarisability and the partial charge can couple to the molecular conformation. These two limitations apply very much to nucleic acids where the charged backbone, anisotropically delocalised electrons in the aromatic bases, polar solvent, and close localisation of cations give a strongly many-body character to the interatomic non-bonded forces.^{4,5}

Although the limitations of classical forcefields are understood, with large discrepancies noted in less-standard conformations such as single stranded DNA⁶, due to the complexity of nucleic acid molecules and the important role of dispersion interactions, it has been quite difficult to arrive at solid quantum benchmark calculations from which to improve these models. Substantial progress has been made in recent years by calculation of dispersion interactions in an explicit many-body manner, working with tensors of directional atom-centred polarisabilities, themselves converged self-consistently with the electron distribution using density-functional theory (for example, in the many-body dispersion method⁷). This approach was found to be quantitative for

DNA stacking energies⁸ and benchmarked favourably against other methods over a dataset of ‘challenging’ noncovalent complexes including DNA bases.⁹

Evaluation of potential energies of static molecular conformations has limited relevance to the highly dynamic finite-temperature behaviour of biomolecules: ideally in order to study large nucleic acid molecules in explicit solvent and salt a potential energy surface (PES) should be defined over the nuclear coordinates. The PES must be differentiable and inexpensive to compute, scaling better than $\mathcal{O}(N^2)$ in the number of atoms. In order to integrate the accuracy of the *ab initio* calculations to existing efficient infrastructure of classical forcefields, a Kernel Modified Molecular Dynamics (KMMD) approach is devised here. The KMMD approach, described in detail below (II), uses a kernel machine to learn not the full PES, but only the part of the quantum correction to the classical PES susceptible to prediction by selected internal degrees of freedom of the nucleic acid chain. Solvent-solvent interactions are thus calculated as usual for the chosen classical forcefield, and solvent-DNA interactions are modified only when they can be predicted by the DNA conformation. To rationalize this, consider that if DNA degrees of freedom predict a void between bases, then the energy to create this void is modified based on the energy to do so in the training data. Because the training data contained some water molecules as well as sodium and DNA, the inter-base dispersion energy is therefore implicitly predicted to include the screening contribution from the amount of water which on average entered the void. DNA-DNA interactions are also only modified in so far as can be predicted from the training data, for instance because information relating to bond lengths was excluded from the training data, bond lengths are only improved in the KMMD as far as they are driven by correlations with the explicitly treated torsions.

Having implemented the KMMD method, simulations were made of a GG-CC DNA complex (with Watson-Crick

^{a)} Also at: Laboratoire de Physique et Chimie Théoriques, Université de Lorraine, Faculté des Sciences et Technologies, Boulevard des Aiguillettes, B.P. 70239, F-54506 Vandoeuvre-les-Nancy, France.

base pairing artificially imposed), under constant force at the O3' and O5' termini, before and after quantum corrections. The observed small reduction in the work to extend with base pairing preserved was consistent with the large long-standing difference between single-molecule stretching experiments on DNA polymers and classical simulation (comparing simulations^{10,11} against a review of experimental data¹², work in experiment is 50-70% of work in classical simulations). While a change in work to extend single steps should imply a change of the same sign for large polymers, for the present prototype study only a small GG·CC complex was studied, and direct experimental measurement of single-step stretching free energies in order to make a quantitative comparison is non trivial. Experimental measurement of single base stacking energy *has* been made for a comparable proxy system, a nicked duplex.¹³ This setup is not exactly equivalent to the calculation geometry however the experimental energies are closer to the KMMD corrected calculation than to the uncorrected (*vide infra*: III).

II. METHODS

A. Generation of DNA Training Data

69 GG·CC DNA dyad structures were sampled from existing classical atomistic simulations of 24bp DNA duplexes at varying extensions documented in previous work.¹⁴ Hydrogens were added to the O5' and O3' ends. Each dyad structure was solvated with 2446 TIP3P waters¹⁵ and two sodium atoms, and the solvent box was then allowed to equilibrate while holding the dyads in stiff restraints for 10ns. This classical simulation and processing was done using AmberTools.¹⁶ The OL15 forcefield¹⁷ was used. Dynamics were classical (no nuclear quantum effects were treated) allowing all atomic masses to be set to 12 amu. From the initial 69 structures, fresh conformations were bootstrapped by long MD simulations (sampling one per ns) to make a training set of 1000 solvated 2bp duplexes.

For each training snapshot, a cluster structure of the DNA plus 20 water molecules and 2 sodium atoms was created. The water molecules were selected based on the 20 closest to any solute atom, this number was found to be sufficient such that backbone charges and solute-solvent hydrogen bonds were always coordinated. Energies were found for the cluster structures using density functional theory (DFT) calculations with the hybrid PBE0 functional^{18–20} for semi-local electron exchange and correlation together with the MBD method^{7,21} for long-range electron correlation interactions (including van der Waals forces). The FHI-aims code was used to converge the electron density,²² with the associated atom-centred basis sets represented at the 'intermediate' level where available (H, C, N, O) but at the 'tight' level when intermediate basis sets were not available for the given element (Na, P). Memory requirement for a neutralised dyad plus 20 water molecules was approximately 12GB, with convergence taking approximately

12 hours on 8 cores. Two structures which did not converge within 72 hours were rejected as having unphysical geometry, leaving 998 initial reference DNA structures for use in the first stage of the machine learning calculation.

B. Kernel Method for Generalisation to PES

The training datapoints $\{\Phi_i(\vec{x}_i)\}$ were defined as the residuals of the quantum and classical energies: $\Phi_i = H_Q(\vec{x}_i) - H_{AMBER}(\vec{x}_i)$. Evaluations of $\{H_{AMBER}\}$ are made at the start of each run, for convenient re-use of the quantum data across forcefields. Feature extraction was carried out in order to reduce the degrees of freedom of the problem, by defining a vector of dihedral angles $\vec{\phi}_i(\vec{x}_i)$ based on the Cartesian coordinates. The canonical DNA torsions ($\alpha, \beta, \gamma, \delta, \epsilon, \zeta, \chi, \nu_0, \nu_1, \nu_2, \nu_3, \nu_4$) were collected, with one occurrence per strand of the backbone torsions $\alpha, \beta, \gamma, \epsilon, \zeta$ and two occurrences per strand of the sugar torsions δ, ν_0-4 and the base twisting angle χ , giving a total of 38 angular degrees of freedom to summarize the state of a base-pair step. These are then (reversibly) expanded to vectors \vec{p}_i of 76 Cartesian degrees of freedom by taking the sin and cos of each angular degree of freedom: $\vec{p}_i = (\sin \vec{\phi}_i, \cos \vec{\phi}_i)$.

The feature space of transformed angles forms a toroidal manifold embedded in \mathbb{R}^{76} . The maximum Euclidean distance between two points is $r_{max} = 2\sqrt{38} \approx 12.3$ and the average distance between two random points is $\sqrt{76} \approx 8.7$. For small angular differences, the distance in feature space is very close to the imaged distance in angular space (perturbing a single angle by 0.1 rad implies $r = 0.0996$ in the feature space, 1 rad implies $r = 0.959$, π rad implies 2). The PES correction at a feature space point \vec{q} is estimated from the training set using a single-parameter Gaussian kernel:

$$\Phi(\vec{q}) = \frac{\sum_i \Phi_i \exp(-\|\vec{q} - \vec{p}_i\|^2 / \sigma^2)}{\sum_i \exp(-\|\vec{q} - \vec{p}_i\|^2 / \sigma^2)} \quad (1)$$

where $\sigma^2 := 0.1$ for all results discussed here. In the limit of small σ the PES becomes a Voronoi diagram in the feature space (losing differentiability), in the limit of large σ the PES becomes flat. For any σ the PES deals gracefully with duplicate training points, simply averaging their contributions: this is valuable because it permits degrees of freedom not represented in the feature space to be averaged over, however the caveat is introduced that if multiple copies of training points exist, untreated degrees of freedom should preferably be sampled using the Gibbs measure at the target temperature for simulation. The denominator in eqn. 1 is treated as an empirical confidence value for a given point evaluation. This kernel method, a minor variation of the extant family of kernel methods, is referred to as a 'Normalised Radial Basis Function' ('nRBF') kernel machine, or equivalently as a nRBF network.²³

Differentiation of the potential to achieve a force is a simple application of the chain and quotient rules, isolating a single torsion ϕ and the single training point $\Phi_0(\phi_0)$ we have:

$$U = \Phi_0 \exp \left[-\frac{1}{\sigma^2} \left[(\sin \phi - \sin \phi_0)^2 + (\cos \phi - \cos \phi_0)^2 \right] \right] / Z \quad (2)$$

where Z is the normalisation factor, the angular force on the torsion is then:

$$-\frac{\partial U}{\partial \phi} = \frac{2U}{\sigma^2} \frac{[\sin \phi \cos \phi_0 - \cos \phi \sin \phi_0] Z + \frac{\sigma^2}{2} \frac{\partial Z}{\partial \phi}}{Z^2} \quad (3)$$

C. Validation of Machine Learning Approach

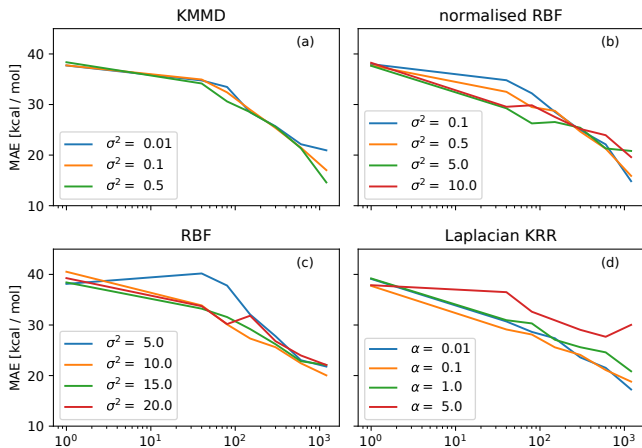


FIG. 1. Validation of KMMD implementation (a) against related machine learning methods, including a conventional nRBF (b) with weights Φ_i as trained parameters. Performance is tested against unseen validation data for increasing amounts of seen training data. The basic KMMD approach is stable with respect to parameters and performs well.

Validation of the KMMD approach was carried out by subsampling a set of 1232 snaps, then evaluating the trained system against the remaining unseen snaps. Mean Absolute Error (MAE) values shown are averages over five independent runs, noise is greater for larger training sets due to the smaller validation sets. The KMMD was robust at predicting energies regardless of the σ^2 parameter and made more efficient use of training data than the other, more sophisticated, approaches. The “normalised Radial Basis Function Network” (nRBF) has an identical functional form to that of the KMMD (eqn. 1) except in that the Φ_i are not training point energies, but arbitrary values fixed by a least-squares fit to the training data.²⁴ In theory this fitting should allow a performance improvement, however with a relatively modest number of training points (as in this example, where the number of centres is still small enough to be computationally cheap at evaluation time), then there is no gain and potentially some minor loss due to under-constraint of the fitting problem. Relaxing the constraint that the weights should be normalised (removing the denominator

of eqn. 1) converts the system to a standard RBF network, this removal of a constraint gives even greater freedom in fitting however no benefit was observed. Kernel Ridge Regression (KRR) is a generalisation of the RBF network which has been used successfully to fit atomisation energies of small molecules *in vacuo* using a feature space constructed around the Coulomb Matrix of atom-atom distances²⁵, the Laplacian kernel $e^{-|x|}$ recommended in this related example was tested in the present feature space and found to perform about as well as the Gaussian nRBF for some choices of the KRR regularisation parameter α . Although the KMMD performed best on the present dataset, all methods have the potential for optimisation and for efficiency gains against larger datasets. In the present examples all training points became nodes of the evaluation, for larger training sets it is possible to merge or prune training points, or even to use non-physical constructed points as RBF centres, gaining efficiency at evaluation time in exchange for a small or zero loss of accuracy.

D. Constant Force Simulations

In order to monitor the influence of extensional force on the DNA dynamics, 36 parallel simulation replicates were prepared with the four terminus atoms G,C@O_{5'},O_{3'} subjected to constant-force restraints of strengths (15, 20, 185, 190) pN, oriented towards fixed sites at the top and bottom of the simulation box. Each replicate was equilibrated in a box of 2446 TIP3P water molecules and 2 sodium ions for 50ns (with a 1fs timestep). During equilibration, frames evaluated with a low confidence (small denominator of eqn. 1) were saved, and those points with the lowest confidence were used to augment the training set to 1232 snaps. In production, force-extension time series were collected for 1500ns per replicate.

The calculation was run with DNA bases restrained to Watson-Crick pairing, following standard B-DNA geometry²⁶ with the intention to therefore focus on the behaviour of stack interactions. In detail the restraints were such that there was no energy penalty for the proton-acceptor pairs G@N₁H-C@N₃, G@NH₂-C@O, C@H₂-G@O to be within distances $\pm 0.2\text{\AA}$ of their equilibrium values, 1.94 \AA , 1.85 \AA , 2.95 \AA . Beyond these ranges, harmonic restraints were imposed with a spring constant of 20 kcal mol⁻¹ \AA^{-2} , for a further 0.5 \AA , after which restraints became constant-force. For the two stronger hydrogen bonds, G@N₁-C@N₃ and C@N-G@O donor-acceptor distance restraints were also added with the same pattern, at equilibrium distances 2.5 \AA and 2.51 \AA , thus (weakly) enforcing planarity of the base pairs.

III. RESULTS

A. Correction versus Multiple Forcefields

Stretching simulations were made against the OL15 force-field, which is considered to be among the best classical DNA models at time of writing²⁷, however it was found prudent to

make a survey of multiple forcefields in order to confirm that the deficiency in treating stacking is general (fig. 2). The *bsc1* forcefield²⁸ was therefore compared against OL15 by post-processing snapshots taken from the KMMD simulations. The DESRES refinement of non-bonded interaction parameters for nucleobases²⁹ was also checked, using the OL15 bonded and other non-specified parameters ('OL15DES').

Firstly snapshots were ordered by the length of the average vector between chain-adjacent bases measured at the N atoms where the chain joins the backbone (fig. 2a), in this case the behaviour around the minimum remained unchanged by adding KMMD, although the potential became apparently stiffer for large separation of the bases. The minimum appeared very sharp with ff99, whether corrected or not, this effect arises because all snaps were generated using OL15+KMMD and are therefore close to the energy minima or valleys as defined by that PES, other forcefields may have similar features but subject to slight geometry shifts, therefore giving apparently stiffer potentials. When lengths x were measured using the terminus atoms O5'-O3' (fig. 2b) an increase in the equilibrium length of the duplex was observed. This shift of $\approx 0.25\text{\AA}$ was independent of the base classical forcefield, and was associated with an continued softening of the potential with respect to further extension. All three forcefields performed similarly for snapshots having small end-to-end length x , at large x the *bsc1* forcefield had the smallest over-estimate of pulling energy. The differences between the forcefields seem to be largely independent of the KMMD correction: all were altered by the KMMD by quite similar amounts.

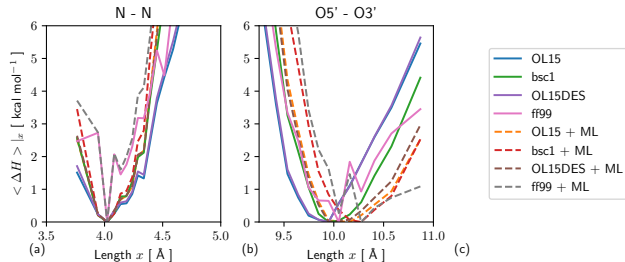


FIG. 2. Postprocessing snaps with different forcefields shows that the differences between them are largely independent of the larger errors fixed by using the KMMD Machine Learning correction (marked as 'ML'). (a): Base-base distance (measured N9-N9 or N1-N1) shows moderate effects, with ML slightly increasing stiffness, but only when far from the minimum. (b): Extension measured between the O5' and O3' termini is noticeably softer after correction, and has a shifted minimum, regardless of the starting forcefield, in a seeming conflict with the tendency of bases to resist having large separation.

B. Modulations of Collective Dynamics

The purpose of the KMMD correction to the forcefield is not primarily to moderate individual dihedral potentials, but

to treat collective interactions in molecules with multiple soft torsions. Fig. 3 compares structural correlations in the DNA duplex under stretch with and without the ML correction. A basic probe of correlation is to collect the proportion of frames in which the χ angles adjacent on the chain were both in the same energy basin (of three available, as determined by the tetrahedral C1' atom at which the base joins the sugar). As expected, the C3:C4 stacked pair of bases has an overall smaller chance for adjacent χ angles to be in the same minimum than does the G1:G2 stack, due to the smaller size of the C base. For both stacks, there is a changeover in the effect of the KMMD with increasing extension: at short extension, KMMD destabilises the base stack relative to standard MD with the OL15 forcefield, while at higher extension, ordering of bases increases for all systems, but especially so with the KMMD (Fig. 3b). This signal is consistent with stabilisation of edge-edge interactions by the KMMD when under imposed extension, as investigated in figures (5, 6).

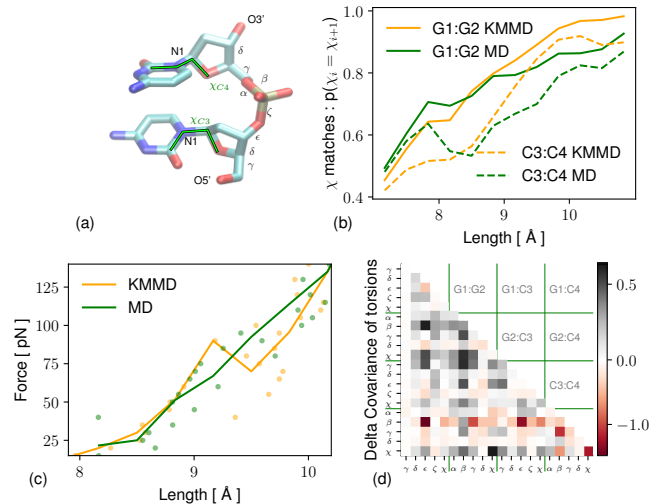


FIG. 3. (a) The CC chain of the GG-CC duplex, with backbone and χ torsions labelled. The four atoms defining each χ are shown with green highlight lines. (b) Base-base interactions versus extension: proportion of χ angles on the same chain to be in the same basin. At short extension, KMMD gives less correlation between adjacent χ , at long extension KMMD strengthens the correlation. (c) Force-extension. Points are independent constant-force simulations; lines are a moving average. (d): Change in covariance of dihedrals, KMMD-MD, over all extensions. Significant signals for χ and for torsions adjacent to central phosphate.

As simulations were run at constant force it is proper to show the force-extension curve (Fig. 3c), although this observable is noisy and subject to finite size effects it does support a reduction of the work to extend the DNA base step, reducing the discrepancy against the lower work to force-melt macroscopic DNA typically seen in experiment relative to simulation. Although the KMMD force-extension trace appears visually to be flatter than the uncorrected trace, an outlier point at 90 pN has the effect of giving almost equal values for the work to extend from 8Å to 10Å when a simple integration is performed using the trapezium rule ($1.69 \text{ kcal mol}^{-1}$

with KMMD versus $1.72 \text{ kcal mol}^{-1}$ without). If the offending datapoint is removed, the corrected work becomes $1.56 \text{ kcal mol}^{-1}$, giving a difference which is still quite small in absolute terms but significant as a fraction of the total work to stretch the base-pair step. The experimental value given by Yakovchuk *et al.*¹³ for the base pair stacking energy of GG-CC at 300K is salt-dependent, giving $1.5 \pm 0.1 \text{ kcal mol}^{-1}$ at a salt concentration of 45mM, equivalent to the selected 2Na^+ in 2446 water.

Fig. 3d gives a sketch of the pairwise torsion angle correlations most affected by the KMMD correction. Covariance $C_{1,2}$ of a pair of dihedrals θ_1, θ_2 is defined here as $(\theta_1 - \bar{\theta}_1)(\theta_2 - \bar{\theta}_2)$ in units radians squared (the means $\bar{\theta}_i$ are found as $\arctan2(\cos \theta_i, \sin \theta_i)$). The (signed) differences in the absolute values of the covariances $|C_{KMMD}| - |C_{MD}|$ are shown in fig. 3d as a heatmap. Overall the KMMD correction promotes disorder (negative delta covariance, orange) however covariance between some torsions is (more weakly) increased (positive delta, grey), in particular involving χ and ζ angles. The β angle linking G bases becomes more covariant (grey) while the β angle linking the C bases becomes much less covariant, and more disordered.

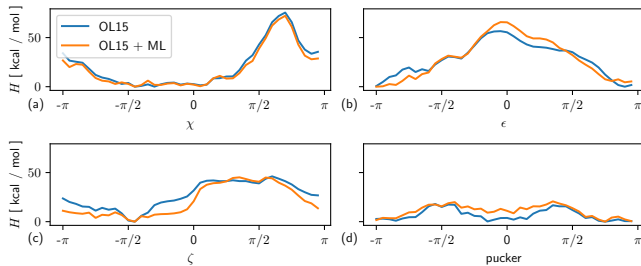


FIG. 4. Averages projected onto key angular degrees of freedom. The χ angle (a) is (overall) well handled without ML, however the sugar pucker and backbone ϵ, ζ torsions (b-d) show substantial deviations.

C. Conformational Analysis

The strength of the ML method is that second-order and higher correlations between torsion angles are treated, however it is still instructive to project onto individual torsions in order to see which conformations of the duplex are stabilised/destabilised relative to classical forcefields. Barriers for rotation in ζ are lower using KMMD than otherwise, barriers in ϵ are higher, while the zero pucker angle ('North') is relatively disfavoured (fig. 4). These data do not imply a simple revision of the existing backbone torsion potentials, not least because the projected-out degrees of freedom are not sampled with respect to the Gibbs measure but rather from an umbrella calculation, however they do show that even if forcefield errors arise from non-bonded forces, they can be predicted to some extent by simultaneous analysis of multiple bond torsions. The example of the steric clash between the hydrogen

attached to the Guanine C8 (or to any purine C8 Hydrogen) and the pentose O4' is investigated by permuting the angles labelled in fig. 5(a). Although the Pauli exclusion which drives the sharp increase of energy as atoms approach overlap is not addressed directly by the KMMD correction; because molecular geometry is determined predominantly by dihedral angles, it is possible to indirectly address a clash which the standard classical treatment misses.

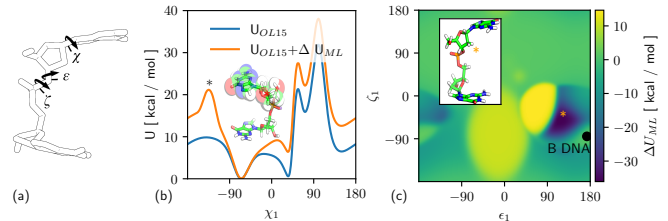


FIG. 5. 1D and 2D cuts holding other angles fixed. (a) Strand 1 (GG) of the dyad, showing angles permuted in the conformation examined. (b) A steric clash (red and white spheres, *inset foreground*) at $\chi = -140^\circ$ is penalised more harshly by the ML method. (c) A highly extended conformation (* and inset) is strongly favoured by the ML.

D. Conformations of Greatest Deviation

Analysing the individual conformations with the greatest differences between KMMD and classical treatment interrogates the limitations of classical methods and helps to motivate the operation of the method. The top 100 structures with large favourable corrections following KMMD are dominated by conformations showing roughly 90° base-base interactions (the single most-favoured conformation is shown in fig. 6).

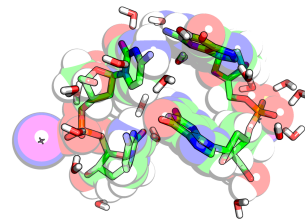


FIG. 6. A conformation highly favoured by the ML relative to the uncorrected OL15 forcefield. Hydrogen bonding is preserved and bases on the same strand remain (sometimes/partly) in contact despite a large vertical stretch.

We refer to stretched duplex geometries with mostly-preserved hydrogen bonding and partly-preserved stacking (subject to tilt and slide) as ' τ -steps'¹⁴, these have been put forward among various candidate geometries for stretched DNA since the earliest molecular mechanics studies³⁰, and linked specifically to stretched GG-CC pairs in recent classical MD work³¹; our primary structural observation into DNA

under tension therefore is that the posited τ -step conformation is confirmed, and that this is very much more favourable than found when modelled classically. The strength of this interaction geometry is not inconsistent with the chemical understanding of 90° interactions between aromatic molecules with hydrogen bonding groups at the edges, in general discussed as ‘remarkably strong’³², although the canonical T-shape aromatic geometry is typically presented as edge-face rather than edge-edge. The lack of directionality imposed by a pointlike treatment of classical atoms leaves little hope of correctly treating the highly directional combination of hydrogen bonding and aromatic stacking in the framework of current mainstream forcefields.

E. Technical Outlook

Distillation of *ab initio* quantum mechanical calculations on fragments into a smooth potential energy surface was successful in this initial example, demonstrating integration of machine-learned physics for short-range interactions with classical modelling of longer-range Coulomb and pairwise dispersion physics, as well as classical treatment of solvent and of stiffer short-range degrees of freedom (bond lengths and angles) not strongly affecting the geometry. Generalisation to long chains as a sum of overlapping fragments does not seem in principle to be a major challenge, nor does generalisation to a wider array of treated repeating units such as amino acids or RNA.

The KMMD concept as described here does ultimately have well-defined limitations, arising in particular from the fact that non-bonded interactions are treated indirectly only. It is entirely feasible to construct an augmented feature space containing two-body or N-body distance information as well as the angular information treated in the present implementation, indeed this has been done for kernel methods targeting smaller molecules,²⁵ however there are always costs for adding complexity. Development of accuracy and generality for kernel-modified MD is likely to continue in the near future by considered design of the feature space in which the kernel operates, and the thoughtful integration of physics which can be calculated cheaply and well from first principles with physics which is best treated through machine learning.

ACKNOWLEDGMENTS

The experiments presented in this paper were carried out using the HPC facilities of the University of Luxembourg³³.

DATA AVAILABILITY STATEMENT

Software to carry out these calculations is available from ambermd.org as a part of the AmberTools 22 package. The dataset of quantum energy evaluations generated for this work is available from the NOMAD materials database.

- ¹F.-Y. Dupradeau, A. Pigache, T. Zaffran, C. Savineau, R. Lelong, N. Grivel, D. Lelong, W. Rosanski, and P. Cieplak, *Phys. Chem. Chem. Phys.* **12**, 7821 (2010).
- ²P. Bleiziffer, K. Schaller, and S. Riniker, *Journal of Chemical Information and Modeling* **58**, 579 (2018).
- ³A. Tkatchenko and M. Scheffler, *Phys. Rev. Lett.* **102**, 073005 (2009).
- ⁴J. Šponer, J. Leszczyński, and P. Hobza, *The Journal of Physical Chemistry* **100**, 5590 (1996).
- ⁵J. Šponer, K. E. Riley, and P. Hobza, *Phys. Chem. Chem. Phys.* **10**, 2595 (2008).
- ⁶C. Nganou, S. D. Kennedy, and D. W. McCamant, *The Journal of Physical Chemistry B* **120**, 1250 (2016).
- ⁷A. Tkatchenko, R. A. DiStasio Jr., R. Car, and M. Scheffler, *Phys. Rev. Lett.* **108**, 236402 (2012).
- ⁸R. A. DiStasio Jr., O. A. von Lilienfeld, and A. Tkatchenko, *Proceedings of the National Academy of Sciences* **109**, 14791 (2012).
- ⁹Y. S. Al-Hamdani and A. Tkatchenko, *The Journal of Chemical Physics* **150**, 010901 (2019).
- ¹⁰S. A. Harris, Z. A. Sands, and C. A. Laughton, *Biophysical journal* **88**, 1684 (2005).
- ¹¹D. R. Roe and A. M. Chaka, *The Journal of Physical Chemistry B* **113**, 15364 (2009).
- ¹²C. Bustamante, S. B. Smith, J. Liphardt, and D. Smith, *Current Opinion in Structural Biology* **10**, 279 (2000).
- ¹³P. Yakovchuk, E. Protozanova, and M. D. Frank-Kamenetskii, *Nucleic acids research* **34**, 564 (2006).
- ¹⁴A. Taghavi, P. van der Schoot, and J. T. Berryman, *Quarterly reviews of biophysics* **50** (2017).
- ¹⁵W. L. Jorgensen, J. Chandrasekhar, J. D. Madura, R. W. Impey, and M. L. Klein, *The Journal of chemical physics* **79**, 926 (1983).
- ¹⁶D. Case, K. Belfon, S. Ben-Shalom, S. Brozell, D. Cerutti, T. Cheatham III, V. Cruzeiro, T. Darden, R. Duke, G. Giambasu, M. Gilson, H. Gohlke, A. Goetz, R. Harris, S. Izadi, S. Izmailov, K. Kasavajhala, A. Kovalenko, R. Krasny, T. Kurtzman, T. LEE, S. LeGrand, P. Li, C. Lin, J. Liu, T. Luchko, R. Luo, V. Man, K. Merz, Y. Miao, O. Mikhailovskii, G. Monard, H. Nguyen, A. Onufriev, F. Pan, S. Pantano, R. Qi, D. Roe, A. Roitberg, C. Sagui, S. Schott-Verdugo, J. Shen, C. Simmerling, N. Skrynnikov, J. Smith, J. Swails, R. Walker, J. Wang, L. Wilson, R. Wolf, X. Wu, Y. Xiong, Y. Xue, D. York, and K. PA, University of California, San Francisco (2020).
- ¹⁷M. Zgarbová, A. M. Rosnik, F. J. Luque, C. Curutchet, and P. Jurečka, *Journal of Computational Chemistry* **36**, 1874 (2015).
- ¹⁸J. P. Perdew, M. Ernzerhof, and K. Burke, *The Journal of Chemical Physics* **105**, 9982 (1996).
- ¹⁹C. Adamo and V. Barone, *The Journal of Chemical Physics* **110**, 6158 (1999).
- ²⁰X. Ren, P. Rinke, V. Blum, J. Wieferink, A. Tkatchenko, A. Sanfilippo, K. Reuter, and M. Scheffler, *New Journal of Physics* **14**, 053020 (2012).
- ²¹A. Ambrosetti, A. M. Reilly, R. A. DiStasio Jr., and A. Tkatchenko, *The Journal of Chemical Physics* **140**, 18A508 (2014).
- ²²V. Blum, R. Gehrke, F. Hanke, P. Havu, V. Havu, X. Ren, K. Reuter, and M. Scheffler, *Computer Physics Communications* **180**, 2175 (2009).
- ²³J. Moody and C. J. Darken, *Neural Comput.* **1**, 281 (1989).
- ²⁴G. Bugmann, *Neurocomputing* **20**, 97 (1998).
- ²⁵K. Hansen, G. Montavon, F. Biegler, S. Fazli, M. Rupp, M. Scheffler, O. A. von Lilienfeld, A. Tkatchenko, and K.-R. Müller, *Journal of Chemical Theory and Computation* **9**, 3404 (2013).
- ²⁶W. Saenger, “Principles of nucleic acid structure,” (Springer, 1984).
- ²⁷P. D. Dans, I. Ivani, G. Portella, C. González, M. Orozco, *et al.*, *Nucleic Acids Research*, gkw1355 (2017).
- ²⁸I. Ivani, P. D. Dans, A. Noy, A. Pérez, I. Faustino, A. Hospital, J. Walther, P. Andrio, R. Goñi, A. Balaceanu, *et al.*, *Nature methods* **13**, 55 (2016).
- ²⁹D. Tan, S. Piana, R. M. Dirks, and D. E. Shaw, *Proceedings of the National Academy of Sciences* **115**, E1346 (2018).
- ³⁰A. Lebrun and R. Lavery, *Nucleic Acids Research* **24**, 2260 (1996).
- ³¹J. W. Shepherd, R. J. Greenall, M. Probert, A. Noy, and M. Leake, *Nucleic Acids Research* **48**, 1748 (2020).
- ³²L. R. Rutledge and S. D. Wetmore, *Journal of Chemical Theory and Computation* **4**, 1768 (2008).

- ³³S. Varrette, P. Bouvry, H. Cartiaux, and F. Georgatos, in *Proc. of the 2014 Intl. Conf. on High Performance Computing & Simulation (HPCS 2014)* (IEEE, Bologna, Italy, 2014) pp. 959–967.